THE JOURNAL OF PHYSICAL CHEMISTRY Letters

pubs.acs.org/JPCL

Letter

Lattice Oxygen Exchange in Rutile IrO_2 during the Oxygen Evolution Reaction

Kevin Schweinar,* Baptiste Gault, Isabelle Mouton, and Olga Kasian*

Cite This: *J. Phys. Chem. Lett.* 2020, 11, 5008−5014

Read Online

ACCESS | Metrics & More | Article Recommendations | Supporting Information

ABSTRACT: The development of efficient acidic water electrolyzers relies on understanding dynamic changes of the Ir-based catalytic surfaces during the oxygen evolution reaction (OER). Such changes include degradation, oxidation, and amorphization processes, each of which somehow affects the material's catalytic performance and durability. Some mechanisms involve the release of oxygen atoms from the oxide's lattice, the extent of which is determined by the structure of the catalyst. While the stability of hydrous Ir oxides suffers from the active participation of lattice oxygen atoms in the OER, rutile IrO_2 is more stable and the lattice oxygen involvement is still under debate due to the insufficient sensitivity of commonly used online electrochemical mass spectrometry. Here, we revisit the case of rutile IrO_2 at the atomic scale by a combination of isotope labeling and atom probe tomography and reveal the exchange of oxygen atoms between the oxide lattice and water. Our approach enables direct visualization of the electrochemically active volume of the catalysts and allows for the estimation of an oxygen exchange rate during the OER that is discussed in view of surface restructuring and subsequent degradation. Our work presents an unprecedented opportunity to quantitatively assess the exchange of surface species during an electrochemical reaction, relevant for the optimization of the long-term stability of catalytic systems.

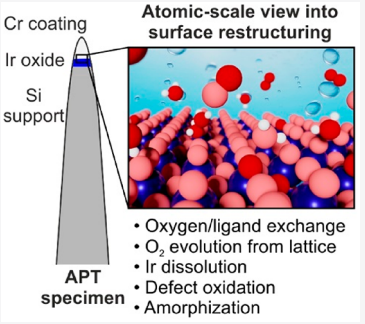

The world's transition toward a more sustainable future relies on innovative solutions for energy conversion and storage. Potential technologies include proton exchange membrane water electrolyzers that can produce carbon-neutral H_2 from water using energy generated by renewable sources.[1,2] However, their technological upscaling is widely hindered by the low efficiency and high costs mainly arising from the low reactivity and instability of catalyst materials. Optimization of the catalyst's performance is especially critical for the anodic oxygen evolution reaction (OER).[3,4] Very few materials can withstand the harsh electrochemical conditions in water electrolyzers, and state-of-the-art devices rely on Ir-based OER catalysts. Ir is scarce, however, and maximizing the durability of Ir-based catalysts requires a fundamental understanding of the mechanisms leading to performance deterioration and structural degradation. A close relationship between the metal cation dissolution and OER activity has long been recognized for several metal oxide catalysts.[5−11] More specifically for Ir oxide, it was shown that at high anodic potentials, the dissolution of Ir and the evolution of oxygen may be linked either through common reaction intermediates[12,13] or via the formation of oxygen molecules from lattice atoms.[10,14] The relative stability of the intermediate products thereby determines the global electrode performance. More recently, it was shown that the formation of a high-valence IrO_3 intermediate contributes to the degradation of thermally prepared IrO_2 catalysts with moderate reactivity, while more reactive Ir-based catalysts dissolve via Ir^{III} intermediates.[12,15] With regard to the stability, the direct participation of the oxygen anion in the oxide lattice in the OER can add to the destabilization of the metal cation that remains behind, resulting in further dissolution.[10]

All processes, the dissolution of metal cations, the evolution of lattice oxygen, or the possible redeposition of dissolved IrO_x species on the surface during the OER renders the top surface amorphous to a certain extent in many catalyst materials,[15−19] resulting in a hydrous, often porous layer with an increased electrochemically active surface area.[18] It is known that the activity and stability of a catalyst strongly depend on its crystal structure,[14,20−24] which also influences the extent of the growth of the hydrous surface layer that exhibits reduced structural order. The structural arrangement of the surface determines the ease of extracting an oxygen anion from the metal oxide lattice, which may subsequently recombine with understoichiometric Ir−O species in the hydrous layer.[10] The removal of oxygen anions from the metal oxide lattice creates vacancies that may destabilize the structure, enable the further growth of the hydrous layer, and accelerate the metal dissolution if the surface is not replenished with another oxygen anion from adsorbed water or the bulk.[25]

Received: April 24, 2020
Accepted: June 4, 2020
Published: June 4, 2020

https://dx.doi.org/10.1021/acs.jpclett.0c01258
J. Phys. Chem. Lett. 2020, 11, 5008−5014

However, even a small degree of exchanged lattice oxygen can potentially affect the structure of the catalyst's surface layer and consequently its long-term performance. This has been a subject of debate in the literature,[3,14,18,26−32] and two key questions must then be answered, i.e., whether lattice oxygen is involved in the OER and whether state-of-the-art analytical tools can capture reaction products with abundances close to their detection limit. The technical limitations could result in erroneous interpretations of the data, i.e., that there is no exchange between lattice oxygen and water in the OER mechanism.

Here, we employ a combination of isotope labeling and atom probe tomography (APT) to re-examine the involvement of lattice oxygen in the OER of reactively sputtered rutile $Ir^{18}O_2$ at a near-atomic scale. In addition, we assess the ligand exchange related to the surface restructuring during reaction. APT allows for the quantification of exchanged ^{18}O for ^{16}O in the near-surface region, which provides evidence for the OER-induced exchange between oxygen atoms from the oxide and water. We present an estimation of the OER-induced lattice oxygen exchange rate and discuss its relevance in view of the structural changes that occur on the catalyst's surface. These aspects are key to understanding the degradation mechanism of metal oxide catalysts during the OER. Our approach presents a new opportunity to investigate phenomena previously unnoticed because of limitations of more traditional analysis techniques, as well as to estimate the electrochemically active volume of the catalyst. The insights can be used for knowledge-based optimization of more sustainable catalysts.

Details about sample preparation, characterization, and experimental methods are presented and discussed in the Supporting Information (section S1 and Figure S1). In brief, isotope-labeled rutile-$Ir^{18}O_2$ films were synthesized by reactive magnetron sputtering in an $^{18}O_2$ atmosphere, which results in the formation of a stoichiometric oxide (see XPS spectra in Figure S2). The proportion of ^{18}O in the total oxygen content in the as-prepared $Ir^{18}O_2$ is 99.6 ± 0.1%. The oxide film features grain sizes in the range of 20−40 nm with a preferential (110) crystal orientation (see XRD spectra in Figure S3). The phase-pure samples were exposed to OER conditions in $H_2{}^{16}O$-based electrolyte using a scanning flow cell connected to an ICP-MS (Figure S1), allowing for the online assessment of Ir dissolution during the electrochemical treatment. After the treatment, the samples were investigated by APT to assess the incorporation of electrolyte-derived ^{16}O into the oxide lattice during the OER.

In line with our previous findings,[14] reactively sputtered $Ir^{18}O_2$ exhibits a high stability when undergoing an anodic polarization treatment, as assessed by the small amount of dissolved Ir. To estimate the oxygen exchange rate, the ^{18}O-labeled electrode was polarized at 1 mA cm^{-2} for 10 min in $H_2{}^{16}O$-based 0.1 M $HClO_4$. The applied protocol was selected on the basis of the OLEMS data obtained on hydrous IrO_x (see section S3 of the Supporting Information).[14] Figure 1 shows the Ir dissolution profile recorded online using ICP-MS. The total amount of dissolved Ir during 10 min of galvanostatic polarization was ∼0.7 ng cm^{-2}. The dissolution profile indicates a decreasing amount of dissolved Ir with time. This trend can even better be seen in Figure S4, where an anodic sweep of potential is performed before and after the galvanostatic polarization. The total amount of dissolved Ir did not exceed 0.9 ng cm^{-2}. Anodic polarization commonly promotes the oxidation and dissolution of lattice defects and

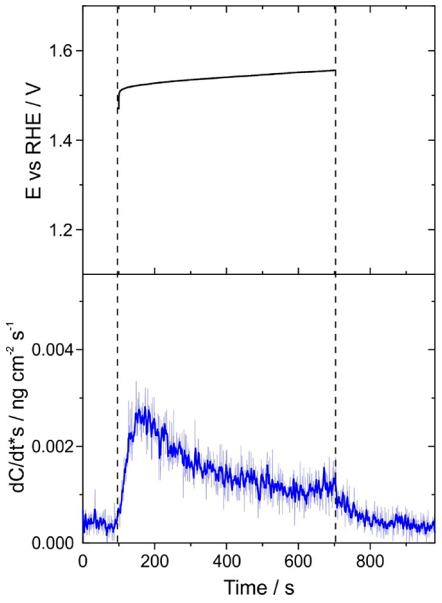

Figure 1. Online observation of Ir dissolution during OER in 0.1 M $HClO_4$ in $H_2{}^{16}O$ during galvanostatic polarization at 1 mA cm^{-2} for 600 s, as measured by the SFC-ICP-MS setup.

results in the overall stabilization of the structure, reflected by the decreasing amount of dissolution products with time, as well as the smaller amount of dissolved Ir during the second sweep of potential (Figure S4c).

A protective Cr layer was deposited on the surface of the sample by electron-beam physical vapor deposition, directly after the electrochemical treatment, ensuring that the top surface of the catalyst was protected from isotopic $^{18}O-^{16}O$ exchange during transport in air. This protection layer enables the APT investigation of the topmost, catalytically relevant atomic layers, as detailed elsewhere.[14,21,33] The three-dimensional (3D) APT reconstruction, in Figure 2a, reveals a significant increase in the level of ^{16}O-containing species toward the surface (red spheres), while the majority of the bulk consists of ^{18}O-containing species (blue spheres). This is further illustrated in the cross-section views in panels b and c of Figure 2, locally reaching 2.5 atom % ^{16}O. Minor lateral variations of ^{16}O are likely related to structural heterogeneities across the catalyst's surface, some of which can become preferential sites for increased levels of degradation and isotope exchange during the reaction.[34] The oxygen atom maps in panels a and b of Figure S7 further evidence the localization of ^{16}O in the near-surface region when compared to ^{18}O, with the localized amount of ^{16}O at the surface strongly exceeding the ^{16}O background observed in the bulk of the sample. The detection limit for ^{16}O was determined to be 89 ppm (for more details, see section S4). Figure 2d presents the percentage of ^{16}O of the sum of all oxygen species [$^{16}O/(^{16}O + {}^{18}O)$]. The profile in Figure 2d considers all ^{16}O-containing species and reveals a significant increase in the level of ^{16}O in approximately the top 2.5 nm of the material (maximum of 4.3%), with an average of 3.5% (±0.7%) of the total oxygen content in the top 0.5 nm. The origin (0 nm on the *x*-axis) in the profile represents the physical surface of the material identified by the adsorbed carbon species (see Figure S7c).[33] A full composition profile is presented in Figure S8. The reported amount of exchanged oxygen should be considered as a

https://dx.doi.org/10.1021/acs.jpclett.0c01258
J. Phys. Chem. Lett. 2020, 11, 5008−5014

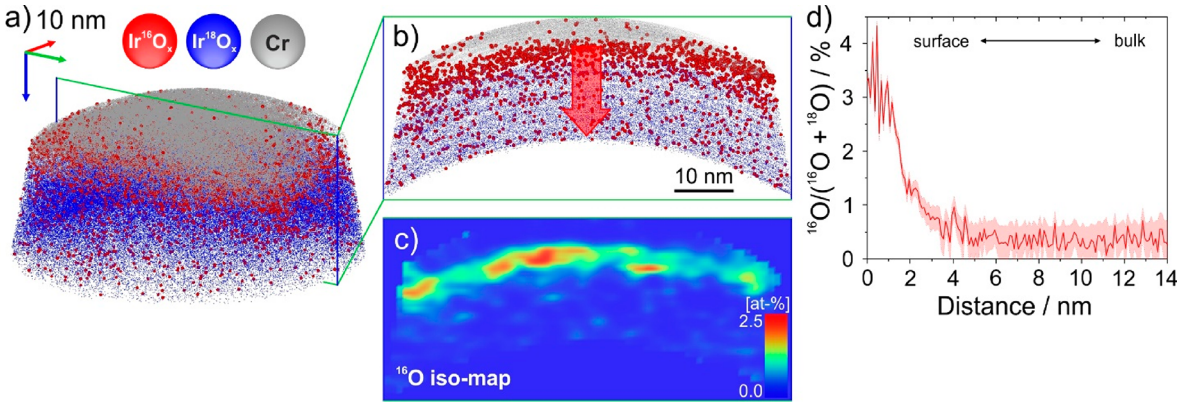

Figure 2. (a) 3D APT reconstruction of the post-OER specimen. The surface is covered with a protective Cr layer enabling the measurement of the topmost atomic layers of the catalyst. The red spheres represent all detected ^{16}O-containing ionic species (red spheres are magnified compared to blue spheres for the sake of clarity). (b) Cross-sectional view onto a 5 nm thick slice through the 3D volume. This view qualitatively shows the enrichment of the near-surface region with electrolyte-derived ^{16}O, indicative of prominent oxygen exchange during the OER. The red arrow depicts the composition profile direction, shown in panel d. The ^{16}O iso-composition map in panel c displays the local accumulation of the exchanged oxygen quantitatively. (d) Depth profile showing the percentage of ^{16}O of the total amount of oxygen.

conservative lower bound, given the experimental limitations of APT, as explained in section S4.

The experimental assessment of isotope exchange rates near room temperature is generally challenging because of their limited magnitude.[35] It was shown for a variety of metal oxides that their oxygen isotope fractionation factor decreases linearly with $1/T^2$ at high temperatures and $1/T$ at low temperatures.[36,37] It is assumed that the hydration of the water−solid interface can accelerate the isotope exchange as compared to the exchange at solid−gas interfaces.[38] Given that the current experiments were performed at room temperature, we consider it reasonable to assume that the observed 3.5% of exchanged oxygen on the surface of the $Ir^{18}O_2$ oxide lattice is a product of the OER, rather than a product of the equilibrium fractionation between the water and the catalyst surface. A discussion of the possible mechanisms that lead to lattice oxygen atom exchange and its implications for the reaction will greatly benefit from the comparison of the amount of exchanged oxygen atoms and evolved O_2 per dissolved Ir atom.

The total amount of dissolved Ir during 10 min of polarization, as shown in Figure 1, was approximately 0.7 ng cm^{-2}. Assuming a covalent radius of Ir of 141 × 10^{-10} cm[39] and a density of IrO_2 of 11.7 g/cm^3, the total amount of dissolved Ir corresponds to roughly 0.2−0.3% of a monolayer (ML). The dissolution rate is approximately 4 × 10^9 atoms cm^{-2} s^{-1}, calculated from the integrated amount of dissolved Ir over time. For the sake of simplicity, we assume two oxygen atoms per Ir atom in a ML of the initial $Ir^{18}O_2$ lattice, of which 3.5% was exchanged for ^{16}O during the OER, according to APT (Figure 2d). This corresponds to roughly 1 × 10^{11} lattice oxygen atoms per second that are directly involved in the OER mechanism. In addition, the number of O_2 molecules evolved during the electrochemical treatment can be calculated from the total current, assuming that Ir dissolution and oxygen evolution are the only processes taking place during the anodic polarization, the former making a negligible contribution to the total current (more details about the calculation are provided in section S7). Under the applied electrochemical conditions, ∼2 × 10^{15} O_2 molecules are evolved per second, comprising predominantly $^{16}O^{16}O$ species formed by the decomposition of water, but possibly also $^{16}O^{18}O$ and $^{18}O^{18}O$ species that contain lattice oxygen atoms.

The involvement of lattice oxygen in the OER mechanism was previously studied mostly through the direct measurement of molecular O_2 evolved from lattice atoms. Most studies combined isotope labeling and differential/online electrochemical mass spectrometry (DEMS/OLEMS) to detect these volatile species. The evolution of oxygen from the lattice was, for instance, evidenced for a series of different catalyst materials, including non-noble perovskites[3,26] and Ni or NiCo[27] in alkaline media, or Au,[28] and sputtered Ru oxide[29] in acidic media. In contrast, there are also reports that lattice oxygen does not participate in acidic OER on RuO_2[30] or alkaline OER on NiFe/NiCoFe.[27] Neither acidic nor alkaline OER on Pt oxide was reported to involve lattice oxygen atoms.[31] Similar studies of Ir oxides are rare, though it was shown that lattice oxygen atoms in Ti/IrO_2 electrodes, synthesized from the thermal decomposition of Ir^{III} salts, are unstable and contribute to the OER.[32] The participation of lattice oxygen atoms was observed for hydrous IrO_x, while IrO_2 prepared by reactive sputtering exhibited high stability toward OER.[18] In a recent study, we correlated the atomic structure of hydrous IrO_x and reactively sputtered rutile-type IrO_2 with differences in the reaction mechanism[14] and stress the need to assess a material's structure and chemistry concomitantly. With a combination of isotope-labeled samples, OLEMS, and ICP-MS, we showed that the stability of rutile IrO_2 strongly exceeds that of hydrous IrO_x, with negligible amounts of dissolved Ir and evolved lattice oxygen under conditions of intense oxygen evolution.

While OLEMS assesses volatile O_2 species evolved during the reaction, APT showcases incorporated, electrolyte-derived ^{16}O in the surface and subsurface regions of the oxide. APT hence allows us to indirectly infer the processes that may contribute to the OER-triggered surface restructuring and degradation of the catalyst, beyond the lattice oxygen evolution. Several processes likely occur concomitantly and lead to an increased level of incorporation of ^{16}O in the structure.

(i) Lattice oxygen atoms contribute to a so-called lattice participation mechanism,[3,11,40] resulting in the evolution of volatile O_2 (i.e., $^{16}O^{18}O$ or $^{18}O^{18}O$ species), as previously observed for hydrous IrO_x (Figure 3a,b).[14,18] Certainly, a limited number of the 1 × 10^{11} lattice oxygen atoms per

https://dx.doi.org/10.1021/acs.jpclett.0c01258
J. Phys. Chem. Lett. 2020, 11, 5008−5014

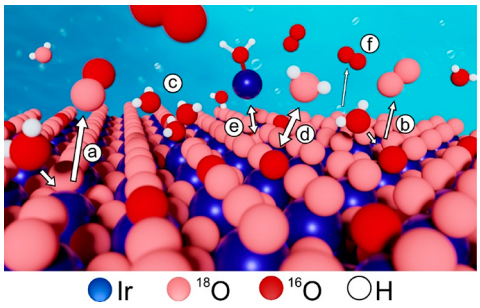

Figure 3. Schematic illustration of processes that involve lattice oxygen atoms occurring on a (001) surface of IrO_2 during OER. The initial oxide lattice is isotope-labeled (i.e., $Ir^{18}O_2$), and the processes shown are representative for experiments performed in a $H_2{}^{16}O$-based electrolyte. All described processes (except f) result in the incorporation of electrolyte-derived ^{16}O in the oxide lattice. (a and b) Example for oxygen evolution involving one or two lattice oxygen atoms. The produced molecules are $^{16}O^{18}O$ and $^{18}O^{18}O$, respectively. In both cases, oxygen vacancies are produced, which can consecutively be replenished by, e.g., the adsorption of water, as indicated in the drawing. (c) Oxidation of surface defects. (d) Isotopic exchange between oxygen atoms of a water molecule and the oxide lattice. (e) Formation of an IrO_x cluster upon dissolution of an Ir^{3+} cation, illustrated by partially formed/broken bonds between $H_2{}^{16}O$ and Ir^{3+}. The formed cluster can subsequently be redeposited on the surface and/or further exchange ligands with the water. (f) The dominant process during the experiment is the evolution of O_2 ($^{16}O^{16}O$), which does not directly involve lattice oxygen atoms.

second, which are being exchanged during the reaction, are evolved as (part of) O_2 molecules. Experimentally, the detection of volatile ^{18}O-containing species is challenging due to the overall small amount of involved lattice oxygen atoms. Hence, high-sensitivity analytics are required. The detection limit for SFC-OLEMS, for example, is reported to be 4×10^{-9} mol cm^{-2} s^{-1} for H_2.[41] Even if the sensitivity for detection of O_2 might be different, the exchanged amount of oxygen from the lattice in this study (1×10^{-13} mol cm^{-2} s^{-1}) is well beyond the detection capabilities of OLEMS. Regardless of the experimental limitations inhibiting a more accurate quantification, oxygen atoms that are removed from the oxide lattice create oxygen vacancies at the surface. The neutralization of the created surface charge imbalance requires the adsorption and incorporation of an oxygen atom from a water molecule, the diffusion of an oxygen atom from the bulk to the surface,[18,25] or the removal of positive charge (i.e., Ir dissolution). The removal and (partial) replenishment of oxygen atoms are likely to increase the extent of structural disorder on the surface (i.e., amorphization).[10,11,21] Similarly, yet without the removal of an oxygen atom from the lattice, the oxidation of inherent oxide defects can result in the incorporation of ^{16}O into the structure, once they become exposed to the electrolyte (Figure 3c).

(ii) ^{18}O atoms from the lattice can simply be exchanged by ^{16}O from the water during the OER (Figure 3d). This exchange may locally be less destructive to the oxide lattice, yet it also requires the metal−oxygen bond to be broken, before another ^{16}O from the water can form a new bond with the undersaturated Ir cation. Given the relatively violent and dynamic nature of the OER under the applied conditions, it is likely that the structural order on the surface will also be disturbed by this process.

(iii) At the applied potential, dissolved Ir ions can be redeposited onto the catalyst's surface and form hydrated $Ir^{16}O_x$ clusters (Figure 3e). In addition, dissolved $Ir^{18}O_x$ clusters from the surface can exchange ligands with water before redeposition. The incorporated ^{16}O atoms through such a ligand exchange reaction represent another possible manner of involvement of a lattice oxygen atom during the OER.

The quantification accuracy of the overall amount of exchanged oxygen could benefit from, e.g., the use of monoisotopic Ir in future experiments (see also section S4). In addition, further development of OLEMS methods is necessary for the direct assessment of evolved lattice oxygen as a volatile compound (i.e., $^{16}O^{18}O$ and $^{18}O^{18}O$) and to understand its contribution to the final amount of exchanged ^{16}O in the lattice.

The APT data in Figure 2d suggest that the top approximately 2.5 ± 0.25 nm of the catalyst was actively involved in the OER, while the material below essentially maintained bulk properties throughout the experiment. The interaction volume reported herein is considerably smaller than for hydrous IrO_x,[14] reflecting the superior stability of rutile IrO_2, given its more compact structure. Our approach, using APT, opens a new opportunity to estimate the electrochemically active volume of an electrocatalyst. Knowing the active near-surface volume of the catalyst can, in principle, be used to develop new design strategies that aim to minimize the amount of Ir used in the first place. In addition, the long-term stability (i.e., Ir dissolution) must also be taken into consideration, as discussed below.

The interaction of lattice oxygen atoms in the OER, in one way or another, inevitably results in structural changes of the catalysts' surface. The rearrangement is accompanied by the dissolution of metal cations from the lattice (see Figure 1) and their partial redeposition, adding to the increasing level of disorder that continuously renders the local stability and reactivity of the catalyst. The current data reveal that one Ir atom is dissolved per ∼33 exchanged lattice oxygen atoms. The electrochemical stability of atoms incorporated in the less crystalline hydrous layer that forms on the surface is expected to be lower than in a highly ordered oxide lattice, due to a lower level of coordination with neighboring atoms and the resulting weaker bonds.[10] In addition, it was shown that the local undercoordination due to an Ir vacancy can result in an electron deficiency on the neighboring oxygen atoms in the lattice, resulting in formally O^{I-} species.[40,42] Concomitantly, excess electrons on defective oxygen atoms can lead to the reduction of neighboring Ir^{IV} to Ir^{III}, increasing the susceptibility of the affected Ir atoms to dissolution.[42,43] Consequently, the metastable Ir^{III} can dissolve without any electron transfer [$Ir^{3+}_{(oxide)} \rightarrow Ir^{3+}_{(aq)}$] or transform into IrO_2.[12] The experimentally observed higher dissolution rate and the participation rate of lattice oxygen atoms in hydrous IrO_x, compared to those of rutile IrO_2, were generally attributed to the higher porosity, the greater abundance of O^{I-} species, -Ir^{III}OOH groups, and a larger number of defects in the former.[14,18,21] As described above, the defects can result in the formation of electrophilic O^{I-} anions that were suggested to be the locus of nucleophilic attack by water, progressing the ongoing degradation process.[42]

Our current data are consistent with the previously reported exceptional stability of reactively sputtered rutile IrO_2 in acidic OER, featuring a stability number (*S*-number) of 8.5×10^5. The *S*-number is a metric to estimate the activity−stability

https://dx.doi.org/10.1021/acs.jpclett.0c01258
J. Phys. Chem. Lett. 2020, 11, 5008−5014

relationship of electrocatalysts independent of the surface area and catalyst loading and equals to the ratio between the amount of evolved O_2 and dissolved iridium.[18] The calculated *S*-number falls in the range of crystalline IrO_2 equivalents ($\sim 8 \times 10^5$ and 1.5×10^7).[18] In addition to previous reports on the material, we can experimentally assess the surface restructuring of rutile IrO_2 during the OER through the incorporation of ^{16}O from the electrolyte into its structure.

Advancing the understanding of degradation mechanisms in the future requires us to systematically address the impact of crystalline defects (i.e., vacancies, dislocations, and grain boundaries) on the dissolution and proposed reaction mechanisms. Just recently, theoretical calculations on IrO_2/RuO_2 have shown that transition metal dopants and structural defects have the ability to alter the OER overpotential favorably and/or render the lattice participation mechanism competitive with the adsorbate evolution mechanism.[44] Furthermore, the understanding of the surface orientation dependence on the reactivity and degradation mechanism must be advanced, as stressed by the pioneering works on RuO_2[30,45−47] and metallic Ir[48,49] for the OER.

In conclusion, the presented approach combining isotope labeling and APT enables the quantification of electrolyte-derived oxygen species incorporated into the oxide lattice during the OER. This number serves as a proxy for the amount of exchanged lattice oxygen atoms arising from different simultaneous degradation mechanisms during the OER. In particular, the OER triggered an exchange of oxygen atoms in the first 2.5 nm (±0.25 nm) of the rutile IrO_2 lattice, which can be crucial in the case of nanoparticles. The restructuring of the surface largely determines the stability of intermediates and resulting pathways of the oxygen evolution and degradation reactions. Surface oxygen exchange kinetics might potentially serve as a stability descriptor in the optimization process of catalysts. More synergistic efforts of theory and experiment are needed to systematically gain advanced insight into fundamental reaction steps that enable an improved knowledge-based catalyst engineering for a more sustainable energy future.

■ ASSOCIATED CONTENT

Supporting Information

The Supporting Information is available free of charge at https://pubs.acs.org/doi/10.1021/acs.jpclett.0c01258.

Experimental methods, sample characterization prior to OER treatment, electrochemical measurements, mass spectrum analysis, atom maps of selected species, full APT composition profile, and details about calculations (PDF)

■ AUTHOR INFORMATION

Corresponding Authors

Kevin Schweinar − *Max-Planck-Institut für Eisenforschung GmbH, Department of Microstructure Physics and Alloy Design, 40237 Düsseldorf, Germany;* orcid.org/0000-0003-1595-2250; Email: k.schweinar@mpie.de

Olga Kasian − *Max-Planck-Institut für Eisenforschung GmbH, Interface Chemistry and Surface Science, 40237 Düsseldorf, Germany; Helmholtz-Zentrum Berlin GmbH, Helmholtz Institut Erlangen-Nürnberg, 14109 Berlin, Germany; Department of Materials Science and Engineering, Friedrich-Alexander-Universität Erlangen-Nürnberg, 91058 Erlangen, Germany;* orcid.org/0000-0001-6315-0637; Email: olga.kasian@helmholtz-berlin.de

Authors

Baptiste Gault − *Max-Planck-Institut für Eisenforschung GmbH, Department of Microstructure Physics and Alloy Design, 40237 Düsseldorf, Germany; Department of Materials, Imperial College London, Royal School of Mines, London SW7 2AZ, U.K.*

Isabelle Mouton − *Max-Planck-Institut für Eisenforschung GmbH, Department of Microstructure Physics and Alloy Design, 40237 Düsseldorf, Germany; CEA Saclay, DES/DMN/Service de Recherches Métallurgiques Appliquées (SRMA), Université Paris-Saclay, 91191 Gif-sur-Yvette, France*

Complete contact information is available at: https://pubs.acs.org/10.1021/acs.jpclett.0c01258

Notes

The authors declare no competing financial interest.

■ ACKNOWLEDGMENTS

K.S. acknowledges the IMPRS-SurMat for funding. U. Tezins, C. Broß, and A. Sturm are acknowledged for their technical support of the FIB & APT facilities at MPIE. O.K. acknowledges support from the Helmholtz-Zentrum Berlin GmbH and from the Helmholtz Association Initiative and Networking Fund. B.G. acknowledges financial support from ERC-CoG-SHINE-771602.

■ REFERENCES

(1) Carmo, M.; Fritz, D. L.; Mergel, J.; Stolten, D. A comprehensive review on PEM water electrolysis. *Int. J. Hydrogen Energy* **2013**, *38* (12), 4901−4934.

(2) Aricò, A. S.; Siracusano, S.; Briguglio, N.; Baglio, V.; Di Blasi, A.; Antonucci, V. Polymer electrolyte membrane water electrolysis: status of technologies and potential applications in combination with renewable power sources. *J. Appl. Electrochem.* **2013**, *43* (2), 107−118.

(3) Grimaud, A.; Diaz-Morales, O.; Han, B.; Hong, W. T.; Lee, Y. L.; Giordano, L.; Stoerzinger, K. A.; Koper, M. T. M.; Shao-Horn, Y. Activating lattice oxygen redox reactions in metal oxides to catalyse oxygen evolution. *Nat. Chem.* **2017**, *9* (5), 457−465.

(4) Binninger, T.; Mohamed, R.; Waltar, K.; Fabbri, E.; Levecque, P.; Kötz, R.; Schmidt, T. J. Thermodynamic explanation of the universal correlation between oxygen evolution activity and corrosion of oxide catalysts. *Sci. Rep.* **2015**, *5* (1), 12167.

(5) Kötz, R.; Stucki, S.; Scherson, D.; Kolb, D. M. In-situ identification of RuO4 as the corrosion product during oxygen evolution on ruthenium in acid media. *J. Electroanal. Chem. Interfacial Electrochem.* **1984**, *172* (1), 211−219.

(6) Cherevko, S.; Zeradjanin, A. R.; Topalov, A. A.; Kulyk, N.; Katsounaros, I.; Mayrhofer, K. J. J. Dissolution of Noble Metals during Oxygen Evolution in Acidic Media. *ChemCatChem* **2014**, *6* (8), 2219−2223.

(7) Chang, S. H.; Danilovic, N.; Chang, K.-C.; Subbaraman, R.; Paulikas, A. P.; Fong, D. D.; Highland, M. J.; Baldo, P. M.; Stamenkovic, V. R.; Freeland, J. W.; Eastman, J. A.; Markovic, N. M. Functional links between stability and reactivity of strontium ruthenate single crystals during oxygen evolution. *Nat. Commun.* **2014**, *5* (1), 4191.

(8) Danilovic, N.; Subbaraman, R.; Chang, K.-C.; Chang, S. H.; Kang, Y. J.; Snyder, J.; Paulikas, A. P.; Strmcnik, D.; Kim, Y.-T.; Myers, D.; Stamenkovic, V. R.; Markovic, N. M. Activity−Stability Trends for the Oxygen Evolution Reaction on Monometallic Oxides in Acidic Environments. *J. Phys. Chem. Lett.* **2014**, *5* (14), 2474−2478.

(9) Reier, T.; Nong, H. N.; Teschner, D.; Schlögl, R.; Strasser, P. Electrocatalytic Oxygen Evolution Reaction in Acidic Environments - Reaction Mechanisms and Catalysts. *Adv. Energy Mater.* **2017**, *7* (1), 1601275.
(10) Binninger, T.; Mohamed, R.; Waltar, K.; Fabbri, E.; Levecque, P.; Kotz, R.; Schmidt, T. J. Thermodynamic explanation of the universal correlation between oxygen evolution activity and corrosion of oxide catalysts. *Sci. Rep.* **2015**, *5*, 12167.
(11) Rong, X.; Parolin, J.; Kolpak, A. M. A Fundamental Relationship between Reaction Mechanism and Stability in Metal Oxide Catalysts for Oxygen Evolution. *ACS Catal.* **2016**, *6* (2), 1153−1158.
(12) Kasian, O.; Grote, J.-P.; Geiger, S.; Cherevko, S.; Mayrhofer, K. J. J. The Common Intermediates of Oxygen Evolution and Dissolution Reactions during Water Electrolysis on Iridium. *Angew. Chem., Int. Ed.* **2018**, *57* (9), 2488−2491.
(13) Kötz, R.; Neff, H.; Stucki, S. Anodic Iridium Oxide Films: XPS-Studies of Oxidation State Changes and. *J. Electrochem. Soc.* **1984**, *131* (1), 72−77.
(14) Kasian, O.; Geiger, S.; Li, T.; Grote, J.-P.; Schweinar, K.; Zhang, S.; Scheu, C.; Raabe, D.; Cherevko, S.; Gault, B.; Mayrhofer, K. J. J. Degradation of iridium oxides via oxygen evolution from the lattice: correlating atomic scale structure with reaction mechanisms. *Energy Environ. Sci.* **2019**, *12* (12), 3548−3555.
(15) Pearce, P. E.; Yang, C.; Iadecola, A.; Rodriguez-Carvajal, J.; Rousse, G.; Dedryvère, R.; Abakumov, A. M.; Giaume, D.; Deschamps, M.; Tarascon, J.-M.; Grimaud, A. Revealing the Reactivity of the Iridium Trioxide Intermediate for the Oxygen Evolution Reaction in Acidic Media. *Chem. Mater.* **2019**, *31* (15), 5845−5855.
(16) May, K. J.; Carlton, C. E.; Stoerzinger, K. A.; Risch, M.; Suntivich, J.; Lee, Y.-L.; Grimaud, A.; Shao-Horn, Y. Influence of Oxygen Evolution during Water Oxidation on the Surface of Perovskite Oxide Catalysts. *J. Phys. Chem. Lett.* **2012**, *3* (22), 3264−3270.
(17) González-Flores, D.; Sánchez, I.; Zaharieva, I.; Klingan, K.; Heidkamp, J.; Chernev, P.; Menezes, P. W.; Driess, M.; Dau, H.; Montero, M. L. Heterogeneous Water Oxidation: Surface Activity versus Amorphization Activation in Cobalt Phosphate Catalysts. *Angew. Chem., Int. Ed.* **2015**, *54* (8), 2472−2476.
(18) Geiger, S.; Kasian, O.; Ledendecker, M.; Pizzutilo, E.; Mingers, A. M.; Fu, W. T.; Diaz-Morales, O.; Li, Z.; Oellers, T.; Fruchter, L.; Ludwig, A.; Mayrhofer, K. J. J.; Koper, M. T. M.; Cherevko, S. The stability number as a metric for electrocatalyst stability benchmarking. *Nature Catalysis* **2018**, *1* (7), 508−515.
(19) Kim, Y.-T.; Lopes, P. P.; Park, S.-A.; Lee, A. Y.; Lim, J.; Lee, H.; Back, S.; Jung, Y.; Danilovic, N.; Stamenkovic, V.; Erlebacher, J.; Snyder, J.; Markovic, N. M. Balancing activity, stability and conductivity of nanoporous core-shell iridium/iridium oxide oxygen evolution catalysts. *Nat. Commun.* **2017**, *8* (1), 1449.
(20) Cherevko, S.; Reier, T.; Zeradjanin, A. R.; Pawolek, Z.; Strasser, P.; Mayrhofer, K. J. J. Stability of nanostructured iridium oxide electrocatalysts during oxygen evolution reaction in acidic environment. *Electrochem. Commun.* **2014**, *48*, 81−85.
(21) Li, T.; Kasian, O.; Cherevko, S.; Zhang, S.; Geiger, S.; Scheu, C.; Felfer, P.; Raabe, D.; Gault, B.; Mayrhofer, K. J. J. Atomic-scale insights into surface species of electrocatalysts in three dimensions. *Nature Catalysis* **2018**, *1* (4), 300−305.
(22) Risch, M.; Grimaud, A.; May, K. J.; Stoerzinger, K. A.; Chen, T. J.; Mansour, A. N.; Shao-Horn, Y. Structural Changes of Cobalt-Based Perovskites upon Water Oxidation Investigated by EXAFS. *J. Phys. Chem. C* **2013**, *117* (17), 8628−8635.
(23) Opalka, D.; Scheurer, C.; Reuter, K. Ab Initio Thermodynamics Insight into the Structural Evolution of Working IrO2 Catalysts in Proton-Exchange Membrane Electrolyzers. *ACS Catal.* **2019**, *9*, 4944−4950.
(24) Zhang, R.; Dubouis, N.; Ben Osman, M.; Yin, W.; Sougrati, M. T.; Corte, D. A.; Giaume, D.; Grimaud, A. A Dissolution/Precipitation Equilibrium on the Surface of Iridium-Based Perovskites Controls Their Activity as Oxygen Evolution Reaction Catalysts in Acidic Media. *Angew. Chem., Int. Ed.* **2019**, *58* (14), 4571−4575.
(25) Grimaud, A.; Demortière, A.; Saubanère, M.; Dachraoui, W.; Duchamp, M.; Doublet, M.-L.; Tarascon, J.-M. Activation of surface oxygen sites on an iridium-based model catalyst for the oxygen evolution reaction. *Nat. Energy* **2017**, *2* (1), 16189.
(26) Yoo, J. S.; Rong, X.; Liu, Y.; Kolpak, A. M. Role of Lattice Oxygen Participation in Understanding Trends in the Oxygen Evolution Reaction on Perovskites. *ACS Catal.* **2018**, *8* (5), 4628−4636.
(27) Lee, S.; Banjac, K.; Lingenfelder, M.; Hu, X. Oxygen Isotope Labeling Experiments Reveal Different Reaction Sites for the Oxygen Evolution Reaction on Nickel and Nickel Iron Oxides. *Angew. Chem., Int. Ed.* **2019**, *58* (30), 10295−10299.
(28) Diaz-Morales, O.; Calle-Vallejo, F.; de Munck, C.; Koper, M. T. M. Electrochemical water splitting by gold: evidence for an oxide decomposition mechanism. *Chemical Science* **2013**, *4* (6), 2334−2343.
(29) Wohlfahrt-Mehrens, M.; Heitbaum, J. Oxygen evolution on Ru and RuO2 electrodes studied using isotope labelling and on-line mass spectrometry. *J. Electroanal. Chem. Interfacial Electrochem.* **1987**, *237* (2), 251−260.
(30) Stoerzinger, K. A.; Diaz-Morales, O.; Kolb, M.; Rao, R. R.; Frydendal, R.; Qiao, L.; Wang, X. R.; Halck, N. B.; Rossmeisl, J.; Hansen, H. A.; Vegge, T.; Stephens, I. E. L.; Koper, M. T. M.; Shao-Horn, Y. Orientation-Dependent Oxygen Evolution on RuO2 without Lattice Exchange. *ACS Energy Letters* **2017**, *2* (4), 876−881.
(31) Willsau, J.; Wolter, O.; Heitbaum, J. Does the oxide layer take part in the oxygen evolution reaction on platinum?: A DEMS study. *J. Electroanal. Chem. Interfacial Electrochem.* **1985**, *195* (2), 299−306.
(32) Fierro, S.; Nagel, T.; Baltruschat, H.; Comninellis, C. Investigation of the oxygen evolution reaction on Ti/IrO2 electrodes using isotope labelling and on-line mass spectrometry. *Electrochem. Commun.* **2007**, *9* (8), 1969−1974.
(33) Schweinar, K.; Nicholls, R. L.; Rajamathi, C. R.; Zeller, P.; Amati, M.; Gregoratti, L.; Raabe, D.; Greiner, M.; Gault, B.; Kasian, O. Probing catalytic surfaces by correlative scanning photoemission electron microscopy and atom probe tomography. *J. Mater. Chem. A* **2020**, *8* (1), 388−400.
(34) Zeradjanin, A. R.; Topalov, A. A.; Van Overmeere, Q.; Cherevko, S.; Chen, X.; Ventosa, E.; Schuhmann, W.; Mayrhofer, K. J. J. Rational design of the electrode morphology for oxygen evolution − enhancing the performance for catalytic water oxidation. *RSC Adv.* **2014**, *4* (19), 9579−9587.
(35) Bottinga, Y.; Javoy, M. Comments on oxygen isotope geothermometry. *Earth Planet. Sci. Lett.* **1973**, *20* (2), 250−265.
(36) Criss, R. E. Temperature dependence of isotopic fractionation factors. In *Stable Isotope Geochemistry*; Tayor, H. P., et al., Eds.; The Geochemical Society: Washington, DC, 1991.
(37) Yong-fei, Z. Calculation of oxygen isotope fractionation in metal oxides. *Geochim. Cosmochim. Acta* **1991**, *55* (8), 2299−2307.
(38) Jehng, J.-M.; Deo, G.; Weckhuysen, B. M.; Wachs, I. E. Effect of water vapor on the molecular structures of supported vanadium oxide catalysts at elevated temperatures. *J. Mol. Catal. A: Chem.* **1996**, *110* (1), 41−54.
(39) Cordero, B.; Gómez, V.; Platero-Prats, A. E.; Revés, M.; Echeverría, J.; Cremades, E.; Barragán, F.; Alvarez, S. Covalent radii revisited. *Dalton Transactions* **2008**, No. 21, 2832−2838.
(40) Pfeifer, V.; Jones, T. E.; Wrabetz, S.; Massué, C.; Velasco Vélez, J. J.; Arrigo, R.; Scherzer, M.; Piccinin, S.; Hävecker, M.; Knop-Gericke, A.; Schlögl, R. Reactive oxygen species in iridium-based OER catalysts. *Chemical Science* **2016**, *7* (11), 6791−6795.
(41) Grote, J.-P.; Zeradjanin, A. R.; Cherevko, S.; Mayrhofer, K. J. J. Coupling of a scanning flow cell with online electrochemical mass spectrometry for screening of reaction selectivity. *Rev. Sci. Instrum.* **2014**, *85* (10), 104101.
(42) Pfeifer, V.; Jones, T. E.; Velasco Velez, J. J.; Massue, C.; Greiner, M. T.; Arrigo, R.; Teschner, D.; Girgsdies, F.; Scherzer, M.; Allan, J.; Hashagen, M.; Weinberg, G.; Piccinin, S.; Havecker, M.; Knop-Gericke, A.; Schlogl, R. The electronic structure of iridium

https://dx.doi.org/10.1021/acs.jpclett.0c01258
J. Phys. Chem. Lett. 2020, 11, 5008−5014

oxide electrodes active in water splitting. *Phys. Chem. Chem. Phys.* **2016**, *18* (4), 2292−6.
(43) Pfeifer, V.; Jones, T. E.; Velasco Vélez, J. J.; Massué, C.; Arrigo, R.; Teschner, D.; Girgsdies, F.; Scherzer, M.; Greiner, M. T.; Allan, J.; Hashagen, M.; Weinberg, G.; Piccinin, S.; Hävecker, M.; Knop-Gericke, A.; Schlögl, R. The electronic structure of iridium and its oxides. *Surf. Interface Anal.* **2016**, *48* (5), 261−273.
(44) Zagalskaya, A.; Alexandrov, V. Role of Defects in the Interplay between Adsorbate Evolving and Lattice Oxygen Mechanisms of Oxygen Evolution Reaction in RuO2 and IrO2. *ACS Catal.* **2020**, *10*, 3650.
(45) Stoerzinger, K. A.; Qiao, L.; Biegalski, M. D.; Shao-Horn, Y. Orientation-Dependent Oxygen Evolution Activities of Rutile IrO2 and RuO2. *J. Phys. Chem. Lett.* **2014**, *5* (10), 1636−41.
(46) Roy, C.; Rao, R. R.; Stoerzinger, K. A.; Hwang, J.; Rossmeisl, J.; Chorkendorff, I.; Shao-Horn, Y.; Stephens, I. E. L. Trends in Activity and Dissolution on RuO2 under Oxygen Evolution Conditions: Particles versus Well-Defined Extended Surfaces. *ACS Energy Letters* **2018**, *3* (9), 2045−2051.
(47) Rao, R. R.; Kolb, M. J.; Hwang, J.; Pedersen, A. F.; Mehta, A.; You, H.; Stoerzinger, K. A.; Feng, Z.; Zhou, H.; Bluhm, H.; Giordano, L.; Stephens, I. E. L.; Shao-Horn, Y. Surface Orientation Dependent Water Dissociation on Rutile Ruthenium Dioxide. *J. Phys. Chem. C* **2018**, *122* (31), 17802−17811.
(48) Özer, E.; Spöri, C.; Reier, T.; Strasser, P. Iridium(1 1 1), Iridium(1 1 0), and Ruthenium(0 0 0 1) Single Crystals as Model Catalysts for the Oxygen Evolution Reaction: Insights into the Electrochemical Oxide Formation and Electrocatalytic Activity. *ChemCatChem* **2017**, *9* (4), 597−603.
(49) Scohy, M.; Abbou, S.; Martin, V.; Gilles, B.; Sibert, E.; Dubau, L.; Maillard, F. Probing Surface Oxide Formation and Dissolution on/of Ir Single Crystals via X-ray Photoelectron Spectroscopy and Inductively-Coupled Plasma Mass Spectrometry. *ACS Catal.* **2019**, *9*, 9859.

https://dx.doi.org/10.1021/acs.jpclett.0c01258
J. Phys. Chem. Lett. 2020, 11, 5008−5014